Improving photon antibunching with two dipole-coupled atoms in whispering-gallery-mode microresonators

Ye Qu,[*] Shuting Shen, Jiahua Li,[†] and Ying Wu[‡]
School of Physics, Huazhong University of Science and Technology, Wuhan 430074, People's Republic of China

(Received 7 September 2019; accepted 17 January 2020; published 7 February 2020)

In the two-atom or multiatom system, the atoms can interact with each other through exchange of virtual photon. This kind of energy exchange is often referred as the dipole-dipole interaction (DDI). Here we consider this DDI system consisting of a pair of two-level atoms strongly coupled with a bimodal whispering-gallery-mode (WGM) microresonator which is driven by an external laser field. Our aim is to explore the photon correlation characteristics of the proposed architecture using realistic experimental parameter values. We compare in detail the quality of photon antibunching (i.e., the smallness of the second-order correlation function) from three involved configurations in cavity quantum electrodynamics (QED): (i) only one two-level atom, (ii) two far apart two-level atoms without DDI, and (iii) two DDI (dipole-coupled) two-level atoms are respectively coupled to the driven WGM microresonator through the evanescent field. We clearly show that the DDI between both atoms can distinctly enhance the photon antibunching even in the weak-coupling regime in configuration (iii) with feature-rich line shapes. We also find that the photon antibunching can be modulated by properly adjusting the atom-cavity coupling strength. In addition, we display that this strong photon antibunching is robust against the cooperative atomic decay. Our DDI-based cavity QED scheme may provide an alternative way to the construction of integrated on-chip single-photon sources.

DOI: 10.1103/PhysRevA.101.023810

I. INTRODUCTION

In recent years, the study of single-photon sources in quantum physics has attracted a great deal of attention due to their potential applications in quantum metrology [1], quantum computation [2,3], quantum simulation [4,5], and quantum communication and networking [6,7], etc. The prefect single-photon sources can be obtained by the physical mechanism of photon blockade, for which a first photon within an optical system blocks the excitation of a second one, corresponding to an orderly output of photons one by one with strong photon antibunching. So far, two types of methods, (1) the conventional photon blockade (CPB) and (2) the unconventional photon blockade (UPB), can be used to produce the photon blockade. The CPB mainly arises from the quantum anharmonicity ladder of energy spectrum that can be introduced via strong nonlinear interactions between single photons. Such a quantum optical phenomenon has been reported in many different architectures within the strong-coupling regime, such as the cavity quantum electrodynamics (QED) systems [8–15], quantum optomechanical systems [16,17], circuit-QED systems [18–20], waveguide-QED systems [21,22], qubit-cavity coupled systems [23], spinning Kerr resonator systems [24], and others. The physical mechanism of the UPB is completely different from that of the CPB described above; nevertheless, it can give rise to strong photon antibunching in the cavity QED even in the presence of much weaker nonlinearities [25]. This achieved strong antibunching is attributed to the destructive quantum interference between different excitation pathways [26–32]. Many studies based on UPB mechanism have been proposed in coupled microcavities with second-order $\chi^{(2)}$ and third-order $\chi^{(3)}$ nonlinearities [33–36], weakly nonlinear photnonic molecules [37], and bimodal QED systems [38,39]. With the improvement of experimental conditions, the UPB has been confirmed experimentally by two different groups [40,41]. These studies open a door towards nonlinear quantum optics at a single-photon level using the weak nonlinear coupling.

Optical microresonators are indispensable tools in both fundamental and applied physics because, on the one hand, they can greatly enhance light-matter interaction and, on the other hand, they can drastically reduce the power necessary to observe strong nonlinear optical phenomena of interest. The most common optical microcavities in quantum optics include conventional the Fabry-Pérot (FP) optical microcavity [8,42,43], whispering-gallery-mode (WGM) microresonator [44,45], photon crystal (PC) nanocavity [46,47], and more. Among them, the WGM microresonators are promising in the multidisciplinary fields such as cavity QED [9,48,49], nonlinear optics [50], quantum optomechanics [51,52], and classical and wave chaos [53,54] owing to their ultrahigh-quality factor (Q) and small mode volume (V). Unlike the standing modes in a conventional FP microcavity, the modes in WGM microresonators are traveling modes. That is to say, the WGM microresonators typically support two counterpropagating modes, i.e., clockwise (CW) and counterclockwise (CCW) propagating modes, with the same polarization and a degenerate frequency. In addition, they allow for massive

[*]ouyeni_92@126.com
[†]Author to whom correspondence should be addressed: huajia_li@163.com
[‡]yingwu2@126.com

production and being integrated on a chip. Largely because of these reasons, optical WGM microresonators often appear in the form of microtoroids [55,56], microspheres [57,58], microrings [59–61], microtubes [62], and microbubbles [63,64] in many diverse areas of fundamental research and applications. Many interesting phenomena, such as nonreciprocal light transmission [65,66], symmetry breaking [67,68], and exceptional points [69,70], have been observed in the WGM microresonators.

Recently, substantial research has been carried out on the system of a single atom localized in the microresonator. As a milestone in this realm, Aoki *et al.* realized the strong coupling between one atom and a monolithic microresonator [48]. Later, by using one atom and a microresonator, an efficient routing of single photons was achieved [49]. Furthermore, strong photon antibunching can occur by placing one dipole quantum emitter in a bimodal WGM microresonator [71]. When two atoms are coupled to the same microresonator, however, the interactions are much more complicated and more physical mechanisms should be considered. The dipole-dipole interaction (DDI) between the two atoms plays an important role in the evolution of the state of the system. When the separation between two atoms is much smaller than the resonance wavelength, the DDI becomes important and cannot be neglected. Effectively, the DDI interaction between the two atoms in the microresonator has found many applications in quantum information processing, for instance, the quantum entanglement [72–74], quantum phase transition [75,76], and DDI-dependent transmission spectrum [77]. To the best of our knowledge, DDI-dependent photon antibunching in the WGM microresonator with two atoms has not been considered much before in theory. With the improvement of experimental conditions, we anticipate that this proposal can become a versatile tool for control of antibunched photons generated in WGM microresonator QED systems.

With this goal in mind, following the quantum models proposed in Refs. [9,48,49,71], we consider a cavity QED system consisting of two dipole-coupled atoms evanescently coupled with a WGM microresonator. We focus on the effect of the DDI between the two atoms on the photon antibunching of the system. In the proposed scheme, the WGM microresonator contains two counterpropagating while coupled optical modes (one CW mode and one CCW mode). One optical mode of the WGM microresonator is coherently driven by an external laser field via an optical tapered fiber waveguide. Using the system parameters that are readily available experimentally, we numerically calculate the equal-time second-order correlation function $g_a^{(2)}(0)$ of one optical mode in the steady state. Taking into account the DDI between the two atoms and working in the weak-coupling regime, the enhancement on the photon antibunching can be achieved when compared to the case that no DDI interaction is included and to the case that only one two-level atom coupled with the WGM microresonator. The weak coupling condition is also favorable since it allows the usage of low-Q microresonators, which are readily realizable in many nanophotonic platforms. Furthermore, we discuss the influence of the atom-cavity coupling strength on the photon antibunching. First, we assume that the coupling strengths of two atoms to the cavity are equal, and then we fix one atom-cavity coupling strength unchanged and alter that of the other one. In both scenarios, the photon antibunching can be enhanced by properly increasing the atom-cavity coupling strength in the presence of the DDI between the two atoms. However, no similar phenomena can be observed when there is no DDI between the two atoms. Finally, we give a brief discussion on the effect of the atomic dissipation induced by the DDI on the system photon statistics and the intracavity photon number. We further prove the robustness of this antibunching and intracavity photon number against the cooperative atomic decay. Our achievable results are useful for the construction of integrated on-chip single-photon sources and enable potential applications in photonic quantum information processing and quantum communications.

The remainder of the paper is organized as follows. In Sec. II the physical model and system Hamiltonian are introduced. In Sec. III first starting from a master equation approach in the rotating-wave approximation and the electric-dipole approximation, we illustrate how to numerically compute the second-order correlation function of the system (Sec. III A). Next, we analyze in detail the influence of interatomic DDI on the photon antibunching in the weak-coupling regime via the second-order correlation function and uncover the DDI-enabled photon antibunching generation in the WGM microresonator with two atoms (Sec. III B). Finally, we summarize our conclusions and offer a brief outlook in Sec. IV. In the Appendix, starting from a Schrödinger equation approach, the insights into the second-order correlation function of the system are presented.

II. PHYSICAL MODEL AND HAMILTONIAN

Figure 1 shows the system schematic diagram of what we consider in this paper. A cavity QED system, consisting of two dipole-coupled two-level atoms interacting with a WGM microresonator through the evanescent field, is side-coupled to a tapered fiber waveguide, in which photons propagate along the arrow direction. The WGM microresonator typically supports two degenerate internal counterpropagating modes [described by operators a (CCW) and b (CW), respectively] with the common frequency ω_C in the absence of scattering [78]. The two two-level atoms (denoted by atom 1 and 2, respectively) with interatomic DDI are coupled to the bimodal WGM microresonator. They interact at rates g_k ($k = 1, 2$) with the internal cavity modes (a and b), which are coupled by scattering of light at a rate h. Each atom has two possible states (a ground state $|g\rangle_k$ and an excited state $|e\rangle_k$) with the same transition frequency ω_A. The atoms play an essential role in controlling the propagation of a single photon. Input to and output from the internal cavity modes of the WGM microresonator are provided by the tapered fiber waveguide, where the external input and output fields of the tapered fiber waveguide are denoted by $\{a_{\rm in}, a_{\rm out}, b_{\rm in}, b_{\rm out}\}$, as shown in Fig. 1. One point we want to emphasize is that only the input field $a_{\rm in}$ is driven by a coherent probe ε_p of frequency ω_p (i.e., $a_{\rm in} = \varepsilon_p e^{-i\omega_p t}$), whereas $b_{\rm in}$ is in a vacuum state (i.e., $b_{\rm in} = 0$). Using the tapered fiber coupler [79], the input field $a_{\rm in} = \varepsilon_p e^{-i\omega_p t}$ can be well guided by the tapered fiber waveguide to drive only the cavity mode a. More information on the device and experimental details have been reported in Refs. [9,48,49,78].

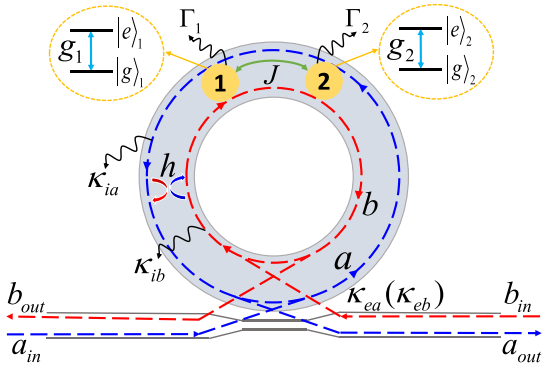

FIG. 1. Schematic diagram of the cavity QED system. It comprises two dipole-coupled two-level atoms with DDI intensity J interacting with a WGM microresonator through the evanescent field. The two two-level atoms, labeled by atoms 1 and 2, are denoted by two yellow dots, respectively. $|g\rangle_k$ (the ground state) and $|e\rangle_k$ (the excited state) are the two possible states of the two two-level atoms with the decay rate Γ_k ($k = 1, 2$). The WGM microresonator contains two degenerate internal counterpropagating modes [labeled by a (CCW) and b (CW), respectively] coupled to a tapered fiber waveguide with the coupling strength κ_{ej}. These cavity modes have intrinsic loss rates κ_{ij} ($j = a, b$) and are coupled to each other at rate h. The $|g\rangle_k \leftrightarrow |e\rangle_k$ transition of the atoms is coupled to the cavity modes (a and b) with the coupling strength g_k. The oval dashed frames show the detailed energy-level structures of the two two-level atoms and the coupling schemes of the two cavity modes. The external input and output fields of the tapered fiber waveguide are described by the symbols $\{a_{\rm in}, a_{\rm out}, b_{\rm in}, b_{\rm out}\}$, respectively.

The overall Hamiltonian for the coherently coupled atom-microresonator compound system under both the rotating-wave and electric-dipole approximations can be written in the form (setting $\hbar = 1$)

$$\begin{aligned}\mathcal{H} = &\sum_{k=1}^{2}[\omega_A\sigma_k^\dagger\sigma_k + g_k(a^\dagger\sigma_k + \sigma_k^\dagger a) + g_k(b^\dagger\sigma_k + \sigma_k^\dagger b)]\\ &+\omega_C(a^\dagger a + b^\dagger b) + h(a^\dagger b + b^\dagger a)\\ &+(\varepsilon_p e^{-i\omega_p t}a^\dagger + \varepsilon_p^* e^{i\omega_p t}a)\\ &+J(\sigma_1^\dagger\sigma_2 + \sigma_2^\dagger\sigma_1),\end{aligned} \tag{1}$$

where the symbols $\sigma_k^\dagger = |e\rangle_k\langle g|$ and $\sigma_k = |g\rangle_k\langle e|$ are the dipole rising and lowering operators for the kth two-level atom, satisfying the fermionic anticommutation relations $\{\sigma_k^\dagger, \sigma_k\} = 1$; a (b) and $a^\dagger$ ($b^\dagger$) are the photon annihilation and creation operators of the two internal cavity modes, satisfying the bosonic commutation relations $[a, a^\dagger] = 1$ and $[b, b^\dagger] = 1$. In Eq. (1), the first term is the unperturbed Hamiltonian of a pair of two-level atoms. The interaction Hamiltonian of the two-level atoms and the cavity modes is shown in the second and third terms. The fourth term represents the energy of the two bare cavity modes a and b. The fifth term accounts for the coherent coupling of the cavity mode a with the cavity mode b, i.e., the so-called mode-coupling term. For the single-side excitation ($a_{\rm in} = \varepsilon_p e^{-i\omega_p t}$ and $b_{\rm in} = 0$) as in our present work, the sixth term describes the driving of the cavity mode a by an external laser field. The remaining term stands for the DDI Hamiltonian between the two two-level atoms. The parameter J is the interatomic DDI coefficient, yielded by

$$J = |\mathbf{d}|^2(1 - 3\cos^2\theta)/|\mathbf{R}|^3, \tag{2}$$

where $|\mathbf{R}|$ is the relative distance between the two two-level atoms and θ is the angle between $\mathbf{R}$ and the atomic dipole moment $\mathbf{d}$. Here we assume that the dipole moments of the two two-level atoms are parallel to each other and are polarized in the direction perpendicular to the interatomic axis. As a result, setting $\cos\theta = 0$ without losing generality, the interatomic DDI coefficient J can be simplified as

$$J = |\mathbf{d}|^2/|\mathbf{R}|^3. \tag{3}$$

Obviously, the interatomic DDI intensity can be adjusted by changing the positions of the two two-level atoms in the WGM microresonator. With the development of the atom trapping and cooling techniques, the two atoms can be trapped at distances on the order of a resonant wavelength, which makes the applicability of DDI between the two atoms feasible [80–83]. Experimentally, the duration of the atom transits is so short that the detection of individual atom positions and their trajectories could not be accomplished in real time [84–86]. In Refs. [48,49,78] cesium atoms are magnetooptically cooled and trapped first, then the atoms fall down freely from the magneto-optical trap and are dropped onto the microresonator, with some cold cesium atoms falling through the evanescent field of the WGMs of the resonator and strongly coupling to the field. The transit time of atoms in the cavity field can last a long time so that there are about 30 atoms passed through the data-collection time window in 10 ms. With the improvement of experimental technology, the duration time for the atoms in the cavity may be long enough to make the measurement and manipulation of atomic positions and trajectories possible. From Eq. (3) one can obtain that the closer the distance between the two two-level atoms is, the stronger the interatomic DDI is. Thus for a theoretically interesting study, one can take readily available experiment parameters to carry out a theoretical study of the DDI-dependent photon antibunching. As a matter of fact, the interatomic DDI has a certain requirement on the distance $|\mathbf{R}|$ (the minimal average interatomic distance of $0.2\lambda_{\rm wavelength}$ [87]; as the distance increases to $0.5\lambda_{\rm wavelength}$ [88], the interatomic DDI is very weak that it can be neglected). For the sake of simplicity, the energy of the atomic ground state $|g\rangle_k$ is set to be zero. Besides these, we drop the hat of the operator in order to keep the notation as simple as possible.

The above system Hamiltonian (1) can be made time-independent by transforming it into the rotating frame at the frequency ω_p of the input driving laser field $a_{\rm in}$. Considering the relationships $\mathcal{H}_0 = \omega_p(a^\dagger a + b^\dagger b + \sigma_1^\dagger\sigma_1 + \sigma_2^\dagger\sigma_2)$, $U(t) = e^{-i\mathcal{H}_0 t} = e^{-i\omega_p t(a^\dagger a + b^\dagger b + \sigma_1^\dagger\sigma_1 + \sigma_2^\dagger\sigma_2)}$, and $\mathcal{H}_{\rm rot} = U^\dagger(t)\mathcal{H}U(t) - iU^\dagger(t)\frac{\partial U(t)}{\partial t} = U^\dagger(t)(\mathcal{H} - \mathcal{H}_0)U(t)$, eventually we can rewrite the Hamiltonian (1) as

$$\begin{aligned}\mathcal{H} = &\sum_{k=1}^{2}[\Delta_A\sigma_k^\dagger\sigma_k + g_k(a^\dagger\sigma_k + \sigma_k^\dagger a) + g_k(b^\dagger\sigma_k + \sigma_k^\dagger b)]\\ &+\Delta_C(a^\dagger a + b^\dagger b) + h(a^\dagger b + b^\dagger a) + \varepsilon_p(a^\dagger + a)\\ &+J(\sigma_1^\dagger\sigma_2 + \sigma_2^\dagger\sigma_1),\end{aligned} \tag{4}$$

where $\Delta_A = \omega_A - \omega_p$ ($\Delta_C = \omega_C - \omega_p$) is the detuning of the input driving laser field frequency ω_p from the two-level atoms transition frequency ω_A (the cavity modes frequency ω_C). Here we consider only the case that the frequencies of the two-level atoms and cavity modes are resonant (i.e., $\omega_A = \omega_C$), thus the same detuning, $\Delta_A = \Delta_C = \Delta$, can be obtained. Without loss of generality, we have taken the driving strength ε_p above to be real.

III. APPROACHES AND DDI-ENABLED PHOTON ANTIBUNCHING GENERATION IN THE WGM MICRORESONATOR

A. Master equation approach and second-order correlation function

To fully describe the system in a more realistic way, loss must be incorporated into the system Hamiltonian. In the current setup, the loss principally results from the cavity field dissipation and the atomic decay, while the atomic decay includes atomic spontaneous emission and cooperative atomic decay. Consequently, the dissipative dynamics evolution of the coupled atom-microresonator compound system can be governed by the master equation [89]

$$\frac{d\rho}{dt} = -i[\mathcal{H}, \rho] + \mathcal{L}[\rho]. \tag{5}$$

Here ρ is the density matrix of the system and $\mathcal{L}[\rho]$ is the whole dissipative Liouvillian superoperator. In our model, the Liouvillian superoperator $\mathcal{L}[\rho]$ can take the following form [73,77]:

$$\mathcal{L}[\rho] = \sum_{j=a}^{b} \mathcal{L}_{\kappa_j}\rho + \sum_{k=1}^{2} \mathcal{L}_{\Gamma_k}\rho + \mathcal{L}_{\gamma_{12}}\rho + \mathcal{L}_{\gamma_{21}}\rho, \tag{6}$$

where

$$\sum_{j=a}^{b} \mathcal{L}_{\kappa_j}\rho = \frac{\kappa_j}{2}(2j\rho j^\dagger - j^\dagger j\rho - \rho j^\dagger j), \tag{7}$$

$$\sum_{k=1}^{2} \mathcal{L}_{\Gamma_k}\rho = \frac{\Gamma_k}{2}(2\sigma_k\rho\sigma_k^\dagger - \sigma_k^\dagger\sigma_k\rho - \rho\sigma_k^\dagger\sigma_k), \tag{8}$$

$$\mathcal{L}_{\gamma_{12}}\rho = \frac{\gamma_{12}}{2}(2\sigma_1\rho\sigma_2^\dagger - \sigma_1^\dagger\sigma_2\rho - \rho\sigma_1^\dagger\sigma_2), \tag{9}$$

$$\mathcal{L}_{\gamma_{21}}\rho = \frac{\gamma_{21}}{2}(2\sigma_2\rho\sigma_1^\dagger - \sigma_2^\dagger\sigma_1\rho - \rho\sigma_2^\dagger\sigma_1). \tag{10}$$

Here Eq. (7) corresponds to the coupling between the two cavity modes (a and b) and the environment, where $\kappa_j = \kappa_{ij} + \kappa_{ej}$ ($j = a, b$) are the total decay rate of the cavity modes. κ_{ij} represents the intrinsic losses rate that is related to the intrinsic quality factor Q_{ij} as $\kappa_{ij} = \omega_C/2Q_{ij}$. Here κ_{ej} describes the extrinsic loss (i.e., the tapered fiber waveguide-resonator coupling) [79,90] relating to the coupling quality factor Q_{ej} as $\kappa_{ej} = \omega_C/2Q_{ej}$. By optimizing material and adjusting the distance between the WGM microresonator and the tapered fiber waveguide, the internal cavity modes can be coupled to the tapered fiber waveguide with relatively high efficiency [79,91]. Equation (8) denotes the coupling of the two two-level atoms to the environment, where Γ_k ($k = 1, 2$) are the decay rate of the atoms. Equations (9) and (10) describe the atom-atom cooperation induced by their coupling with a common vacuum bath [72,73,92], where γ_{12} and γ_{21} are the DDI-induced decay (i.e., the cooperative atomic decay). When the distance between the two two-level atoms is small relative to the radiation wavelength $\lambda_{\text{wavelength}}$ (i.e., $0.2\lambda_{\text{wavelength}} \leqslant |\mathbf{R}| \leqslant |0.5\lambda_{\text{wavelength}}$) [87,88], the cooperative atomic decays γ_{12} and γ_{21} need to be taken into account in the system. In general, when $\gamma_{12} \ll \Gamma_1$ ($\gamma_{21} \ll \Gamma_2$) is satisfied, it can be ignored. In this paper, we primarily focus on the effect of the interatomic DDI on the statistical properties of the cavity mode a, which can be distinguished by the second-order correlation function

$$g_a^{(2)}(\tau) = \frac{\langle a^\dagger(0)a^\dagger(\tau)a(\tau)a(0)\rangle}{\langle a^\dagger(0)a(0)\rangle^2}, \tag{11}$$

where τ is the time delay for the two different photons arriving at the detector. Then the photon statistical properties of the cavity mode a can be well distinguished according to the value of $g_a^{(2)}(\tau)$ at the zero-time delay. More concretely, the value of $g_a^{(2)}(0) < 1$ [$g_a^{(2)}(0) > 1$] corresponds to sub-Poisson (or super-Poisson) statistics of the cavity mode a, which is a nonclassical (classical) effect. This effect of the sub-Poisson (or super-Poisson) statistics is often referred to as photon antibunching (or bunching). The single-photon regime is usually characterized by $g_a^{(2)}(0) < 0.5$, while $g_a^{(2)}(0) \to 0$ indicates complete photon blockade. For a fully quantum mechanical treatment of the coherently coupled atom-microresonator compound system, we can compute numerical solutions to the full master equation [see Eq. (5)] using truncated number state bases for both cavity modes. In this way, the steady-state density matrix ρ_{ss} (i.e., $d\rho/dt = 0$) can be obtained, and then the average value of arbitrary operator O can be calculated as $\langle O\rangle = \text{Tr}(\rho_{ss}O)$. Under this operation, the steady-state value of the zero-delay-time second-order correlation function $g_a^{(2)}(0)$ can be easily found as

$$g_a^{(2)}(0) = \frac{\text{Tr}(\rho_{ss}a^\dagger a^\dagger aa)}{[\text{Tr}(\rho_{ss}a^\dagger a)]^2}. \tag{12}$$

Finally, the measurement of the equal-time second-order correlation function $g_a^{(2)}(0)$ can be performed by employing the well-known Hanbury-Brown-Twiss (HBT) device [93].

On the other hand, starting from a Schrödinger equation approach, insights into the second-order correlation function of the system are also provided (see the Appendix). The gained insights contribute to a better understanding of how the second-order correlation function $g_a^{(2)}(0)$ is regulated by the system parameters. Because the two-atom system, to some extent, is analogous to the one-atom system, we make use of the system parameters in the numerical simulations all coming from the experiment [9], in which a photon turnstile dynamically regulated by a single atom within the WGM microresonator is achieved. The detailed numerical simulation results are presented in Figs. 2–7 below.

B. Results of numerical calculation and in-depth discussion of the equal-time second-order correlation function

Different from the previous studies where only one two-level atom is coupled to the WGM microresonator [9,48,49,71], two two-level atoms interact simultaneously with the WGM microresonator in our proposed scheme.

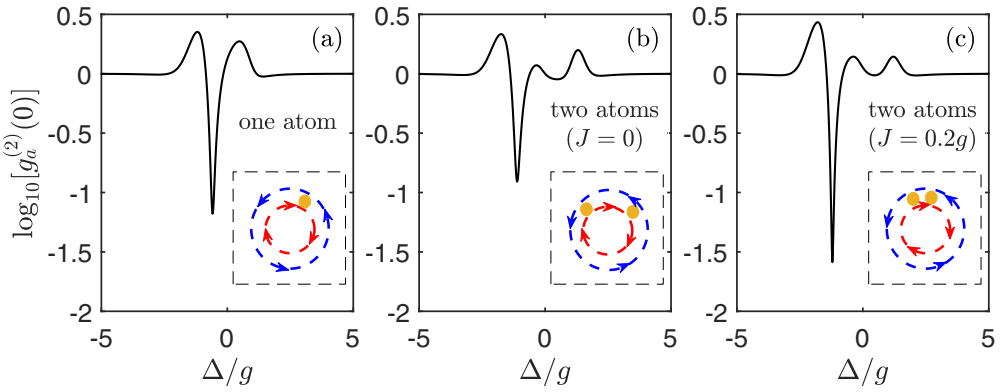

FIG. 2. The equal-time second-order correlation function of the cavity mode a on a logarithmic scale, i.e., $\log_{10}[g_a^{(2)}(0)]$ as a function of the laser detuning Δ for three different configurations in cavity QED: (a) only one two-level atom is coupled to the WGM microresonator; (b) two far apart separated two-level atoms (the interatomic DDI strength $J = 0$) interact with the WGM microresonator; and (c) two dipole-coupled two-level atoms (with interatomic DDI strength $J = 0.2g$) are coupled with the WGM microresonator. Panels (a)–(c) display that the presence of DDI increases the depth of the photon blockade. All other system parameters used here are set as follows: $\kappa_{ia}/2\pi = \kappa_{ib}/2\pi = 75$ MHz, $\kappa_{ea}/2\pi = \kappa_{eb}/2\pi = 90$ MHz, $\Gamma_1/2\pi = \Gamma_2/2\pi = 5.2$ MHz, $\gamma_{12}/2\pi = \gamma_{21}/2\pi = 0$, $h/2\pi = 50$ MHz, $g_1 = g_2 = g$, $g/2\pi = 70$ MHz, and $\varepsilon_p/2\pi = 7$ MHz, respectively. The parameter values are chosen to be in accordance with a relevant experiment in a photon turnstile [9].

Hence the interatomic coupling should be considered, especially for the case that the distances between the two atoms are comparable to the resonance wavelength. In this scenario, the interatomic DDI plays an important role in the evolution of the state of the whole system. This can cause the atoms to move or rapidly oscillate around their equilibrium positions, and profoundly affect the light absorption and lead to the shift of the atomic energy levels [76,77].

To this end, it is worthwhile completely exploring the influence of the interatomic DDI on the statistical properties of the system. For a better comparison in this part, Fig. 2 displays the equal-time second-order correlation function $g_a^{(2)}(0)$ of the cavity mode a on a logarithmic scale $\log_{10}[g_a^{(2)}(0)]$ as a function of the laser detuning Δ under the three involved configurations: (1) only one two-level atom is coupled to the WGM microresonator; (2) two far apart two-level atoms (without interatomic DDI strength $J = 0$) interact with the WGM microresonator; and (3) two dipole-coupled two-level atoms (with interatomic DDI strength $J = 0.2g$) are coupled with the WGM microresonator. In order to understand these three situations more intuitively, we offer the three simple sketches within the dashed frames in the insets of Fig. 2. We consider first the simplest case that the WGM microresonator contains only one two-level atom without introducing another additional atom. As displayed in Fig. 2(a), the profile of the equal-time second-order correlation function $g_a^{(2)}(0)$ on a logarithmic scale $\log_{10}[g_a^{(2)}(0)]$ varying with the laser detuning Δ exhibits a peak-dip-peak structure. The value of the equal-time second-order correlation function $\log_{10}[g_a^{(2)}(0)]$ at the dip is about -1.18 [i.e., $g_a^{(2)}(0) < 1$]. Physically, the value of $\log_{10}[g_a^{(2)}(0)]$ is closely related to the photon statistics. Specifically, $\log_{10}[g_a^{(2)}(0)] < 0$ refers to the photon antibunching, which corresponds to sub-Poisson photon statistics, the photon blockade happens, and single photons come out of the WGM microresonator. However, $\log_{10}[g_a^{(2)}(0)] > 0$ stands for the photon bunching, photons inside the WGM microresonator enhance the resonantly entering probability of subsequent photons, and, namely, the super-Poisson photon statistics occurs. Thus from the plot in Fig. 2(a), the photon antibunching can be observed in the cavity mode a when there is only one two-level atom coupled to the WGM microresonator.

In order to further illustrate the interatomic interactions, an additional two-level atom needs to be added in the WGM microresonator. For the case of two atoms, how the location of the newly input atom, i.e., the relative distance $|\mathbf{R}|$ between the two atoms, modifies the photon statistics of the system is of great concern to us. As has been mentioned before, the strength of the interatomic DDI depends sensitively on the relative distance $|\mathbf{R}|$ between the two two-level atoms. In the range of $0.2\lambda_{\text{wavelength}} \leqslant |\mathbf{R}| \leqslant 0.5\lambda_{\text{wavelength}}$, the intensity of DDI between the two two-level atoms gradually decreases with the increase of the relative distance $|\mathbf{R}|$. As is shown in the dashed frames of Fig. 2(b), the DDI between the two atoms can be neglected ($J = 0$) when the distance between the two atoms is far in the WGM microresonator. In Fig. 2(b), the profile of the equal-time second-order correlation function $g_a^{(2)}(0)$ on a logarithmic scale $\log_{10}[g_a^{(2)}(0)]$ exhibits a peak-dip-peak-dip-peak structure instead of a peak-dip-peak structure. Meanwhile, it can be clearly seen that the value of the minimum dip in Fig. 2(b) is shallower than that in Fig. 2(a), but it is still negative. This means that the photon antibunching can still be observed in the cavity mode a when the WGM microresonator contains the two two-level atoms without the interatomic DDI. Compared with the case of only one two-level atom in Fig. 2(a), the photon antibunching of the cavity mode a in Fig. 2(b) is obviously weakened. From a physical standpoint, this is because the additional dissipative pathways are introduced by the other atom-microresonator coupling.

An interesting question is What can happen when the DDI between the two atoms works? In order to investigate the effect of DDI on the photon statistical properties, one can change the distance between the two atoms so that DDI can function. In the dashed frames of Fig. 2(c), the distance between the two atoms is assumed to be shortened significantly

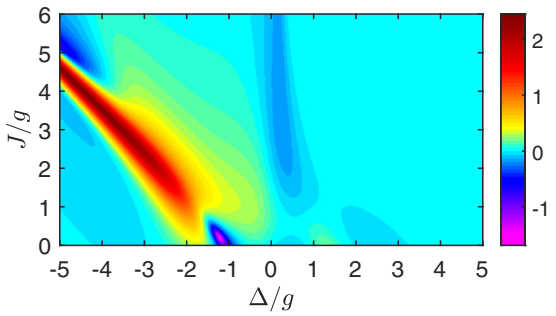

FIG. 3. Contour plot of the equal-time second-order correlation function of the cavity mode a on a logarithmic scale $\log_{10}[g_a^{(2)}(0)]$ as a function of the laser detuning Δ and the interatomic DDI strength J for the case of a pair of two-level atoms simultaneously coupled to the WGM microresonator. The other system parameters used here are set as follows: $\kappa_{ia}/2\pi = \kappa_{ib}/2\pi = 75$ MHz, $\kappa_{ea}/2\pi = \kappa_{eb}/2\pi = 90$ MHz, $\Gamma_1/2\pi = \Gamma_2/2\pi = 5.2$ MHz, $\gamma_{12}/2\pi = \gamma_{21}/2\pi = 0$, $h/2\pi = 50$ MHz, $g_1 = g_2 = g$, $g/2\pi = 70$ MHz, and $\varepsilon_p/2\pi = 7$ MHz, respectively.

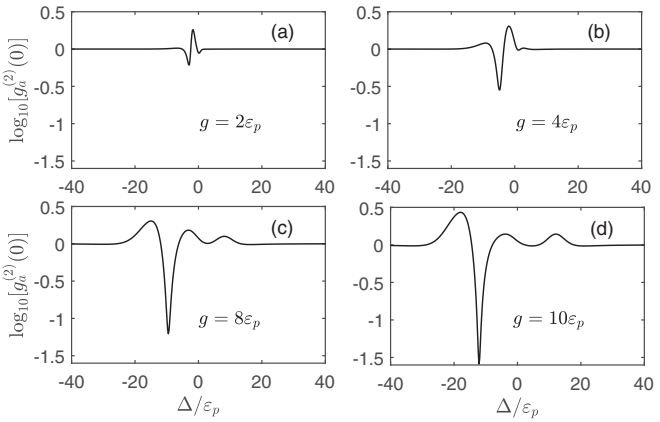

FIG. 4. The equal-time second-order correlation function of the cavity mode a on a logarithmic scale $\log_{10}[g_a^{(2)}(0)]$ as a function of the laser detuning Δ for four different values of the atom-cavity coupling strength g when considering the interatomic DDI strength $J/2\pi = 14$ MHz. The other system parameters used here are set as follows: $\kappa_{ia}/2\pi = \kappa_{ib}/2\pi = 75$ MHz, $\kappa_{ea}/2\pi = \kappa_{eb}/2\pi = 90$ MHz, $\Gamma_1/2\pi = \Gamma_2/2\pi = 5.2$ MHz, $\gamma_{12}/2\pi = \gamma_{21}/2\pi = 0$, $h/2\pi = 50$ MHz, $g_1 = g_2 = g$, and $\varepsilon_p/2\pi = 7$ MHz, respectively.

when compared with that in Fig. 2(b). It means that in this case the two DDI (dipole-coupled) atoms are placed in the WGM microresonator. As is clearly shown in Fig. 2(c), the line shape of the equal-time second-order correlation function $g_a^{(2)}(0)$ on a logarithmic scale $\log_{10}[g_a^{(2)}(0)]$ is similar to that in Fig. 2(b). In Fig. 2(c), however, one can easily see that the first dip considerably deepens, which indicates that the photon antibunching effect is significantly enhanced. It reveals that the interatomic DDI can enhance the photon antibunching effect. More interestingly, the value of the minimum dip in Fig. 2(c) is much smaller than that in Fig. 2(a). Generally speaking, the photon antibunching can occur when the value of the equal-time second-order correlation function $g_a^{(2)}(0)$ on a logarithmic scale $\log_{10}[g_a^{(2)}(0)]$ is negative. The smaller the value is, the stronger the photon antibunching is. Combining Figs. 2(a), 2(b), and 2(c), we can arrive at the conclusion that the photon antibunching can be manipulated and optimized by adjusting the DDI between the two atoms (i.e., the relative distance between the two atoms) when there are two two-level atoms simultaneously coupled to the cavity field.

As has been discussed above, the DDI between the atoms has a great influence on the photon antibunching for the case of two two-level atoms coupled to the WGM microresonator. At the same time, the interatomic DDI can be adjusted by changing the relative distance between the two atoms. It suggests that the result can provide another parameter for us to adjust photon statistical properties. In order to better understand the effect of the interatomic DDI on the photon antibunching, the equal-time second-order correlation function $g_a^{(2)}(0)$ on a logarithmic scale $\log_{10}[g_a^{(2)}(0)]$ is plotted in Fig. 3 as a function of the laser detuning Δ and the interatomic DDI strength J for the case of two atoms. From Fig. 3, we can see that the value of $\log_{10}[g_a^{(2)}(0)]$ can be tuned to be positive or negative with the adjustment of the laser detuning and the interatomic DDI strength within the given parameter range. One can find that the cavity mode a exhibits strong bunching photon statistics (corresponding to the dark red area) and strong antibunching photon statistics (corresponding to the magenta area) for the negative detuning, i.e., $\Delta < 0$. Compared with the case of $\Delta < 0$, both the bunching and the antibunching photon statistics are obviously weakened no matter how one changes the relative distance between the two atoms when the detuning is positive, namely, $\Delta > 0$. It indicates that the value of $\log_{10}[g_a^{(2)}(0)]$ is more sensitive to the interatomic DDI in the negative detuning regime. The numerical results provide important information that the photon statistics of the cavity mode a indeed is affected by the interatomic DDI. The strong antibunching or bunching photon statistics can be generated by perfectly matching the interatomic DDI strength J and the laser detuning Δ (cf. Fig. 3).

In all the analysis above, we have shown that the interatomic DDI affects the photon statistics of the system greatly. One can use it to enhance the photon antibunching. However, optimized photon antibunching can be observed only with the other system parameters well chosen, as has been displayed in Fig. 3, where the laser detuning Δ must be well selected to obtain the smallest $\log_{10}[g_a^{(2)}(0)]$. Interestingly, we shall show that the atom-cavity coupling can also have great impact on the system photon statistics when DDI exists. From Eq. (3), we know that the DDI intensity between the two atoms depends only on the relative positions of the two atoms in the WGM microresonator. In practice, the coupling strength of the two atoms to the cavity modes is also position-dependent. In addition, it is also related to the radial distance of the atoms from the surface of the toroid and the vertical coordinate along the symmetry axis [9,48]. In the presence of DDI between the two atoms, the equal-time second-order correlation functions $g_a^{(2)}(0)$ on a logarithmic scale $\log_{10}[g_a^{(2)}(0)]$ as a function of the laser detuning Δ with different atom-cavity coupling strengths g are plotted in Fig. 4. For simplicity of discussion, we set the atom-cavity coupling strengths for both atom 1 and atom 2 to be equal, namely, $g_1 = g_2 = g$. It can be seen from Fig. 4(a) for the case of $g = 2\varepsilon_p$ (i.e., $g/2\pi = 14$ MHz) that the profile of the equal-time second-order correlation function $g_a^{(2)}(0)$ on a logarithmic scale $\log_{10}[g_a^{(2)}(0)]$ is a narrow

dip-peak structure that is similar to the asymmetric Fano-like line shape [94,95]. The value of the dip in Fig. 4(a) is about -0.21, which means that the photon antibunching effect is significantly weak. With the atom-cavity coupling strength increasing, the profile of $\log_{10}[g_a^{(2)}(0)]$ is still an asymmetric Fano-like line shape, but the dip in Fig. 4(b) becomes deeper and the value is approximately -0.55. However, the profile of $\log_{10}[g_a^{(2)}(0)]$ in Figs. 4(c) and 4(d) changes evidently as the coupling strength g increases. In Figs. 4(c) and 4(d), the number of the dips and peaks increases. The most noticeable change is that the minimum dip in the profile of $\log_{10}[g_a^{(2)}(0)]$ becomes deeper and deeper with the increase of the atom-cavity coupling strength. Thus, from these results of Fig. 4, we can conclude that the photon antibunching effect can be enhanced by properly increasing the atom-cavity coupling strength with the consideration of the interatomic DDI.

In all the above considerations, we have assumed that the coupling strengths of the two atoms to the cavity modes are equal [73,76,77,96]. For the case of a pair of two-level atoms simultaneously coupled to an optical cavity, the two atoms usually no longer possess the equivalent coupling strengths to the cavity modes. In Refs. [97,98], the case of different atom-cavity coupling constants is considered, but the interatomic DDI is neglected. Thus it is both practical and interesting to consider the effects of the unequal atom-cavity coupling, i.e., $g_1 \neq g_2$, on the photon statistical properties, especially in the presence of DDI. In the current system, when there are two atoms in the WGM microresonator, the equal-time second-order correlation function $g_a^{(2)}(0)$ on a logarithmic scale $\log_{10}[g_a^{(2)}(0)]$ as a function of the laser detuning Δ with different atom-cavity coupling strengths g_2 is plotted in Figs. 5(a)–5(h). Moreover, in order to have a contrast between the absence and presence of the interatomic DDI, $J = 0$ is set in Figs. 5(a)–5(d) and $J = 0.2g_1$ is set in Figs. 5(e)–5(h), respectively. When there is no DDI between the two atoms, it can be seen from Figs. 5(a)–5(d) that the profiles of $\log_{10}[g_a^{(2)}(0)]$ have only slight changes with the enhancement of the atom-cavity coupling strength g_2. Concretely, as the coupling strength varies from $g_2 = 0.3g_1$ to $g_2 = 0.5g_1$, the value of the minimum dip in the profile changes from -0.99 to -0.70. Obviously, the photon antibunching becomes weaker with the increase of the coupling strength g_2. Similar phenomena can also be observed in Fig. 5(c). When $g_2 = 0.7g_1$ in Fig. 5(c), the value of the minimum dip reaches -0.68. However, with a further increase in the coupling strength g_2, e.g., $g_2 = 0.9g_1$ in Fig. 5(d), the minimum dip in the profile becomes deeper compared to that of Fig. 5(c), and the value of the minimum dip in Fig. 5(d) is about -0.82. So from Figs. 5(a)–5(d), the tendency of the minimum values for $\log_{10}[g_a^{(2)}(0)]$ does not change monotonously with the increase of the coupling strength g_2 for the case of $J = 0$. Meanwhile, this result can be well verified by Fig. 6(a) which presents the color-scale two-dimensional map of the equal-time second-order correlation function $g_a^{(2)}(0)$ on a logarithmic scale $\log_{10}[g_a^{(2)}(0)]$ as a function of the coupling strength g_2 and the laser detuning Δ for $J = 0$. From Fig. 6(a), one can clearly see that photon antibunching can be established in the cavity mode a in between the red regions. The blue area in Fig. 6(a) corresponds exactly to the minimum dip in Figs. 5(a)–5(d). Comparing Fig. 6(a) and Figs. 5(a)–5(d), we

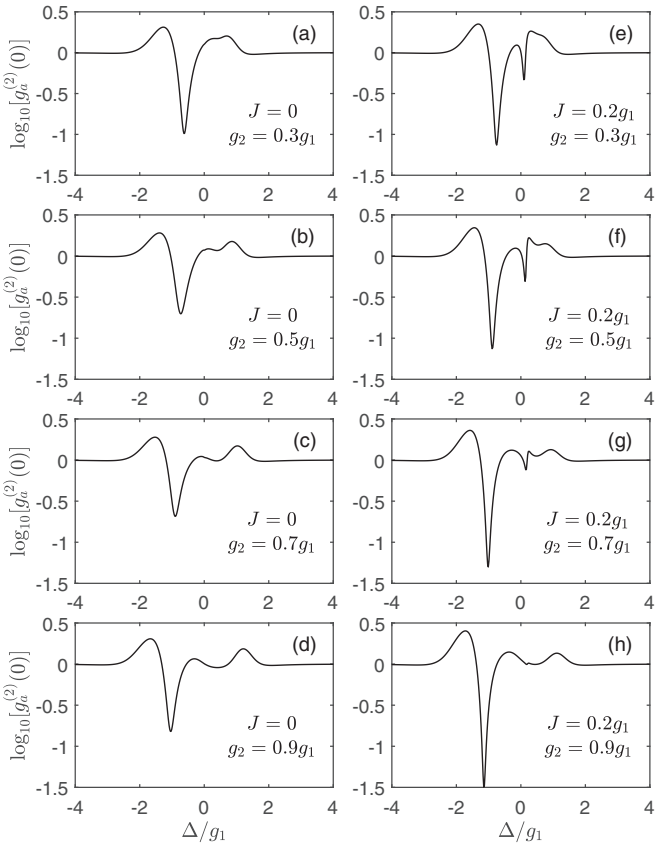

FIG. 5. The equal-time second-order correlation function of the cavity mode a on a logarithmic scale $\log_{10}[g_a^{(2)}(0)]$ as a function of the laser detuning Δ for four different values of the atom-cavity coupling strength g_2 without and with interatomic DDI. Panels (a)–(d) and (e)–(h) correspond, respectively, to $J = 0$ (without interatomic DDI) and $J = 0.2g_1$ (with interatomic DDI, i.e., $J/2\pi = 14$ MHz). The other system parameters used here are set as follows: $\kappa_{ia}/2\pi = \kappa_{ib}/2\pi = 75$ MHz, $\kappa_{ea}/2\pi = \kappa_{eb}/2\pi = 90$ MHz, $\Gamma_1/2\pi = \Gamma_2/2\pi = 5.2$ MHz, $\gamma_{12}/2\pi = \gamma_{21}/2\pi = 0$, $h/2\pi = 50$ MHz, $g_1/2\pi = 70$ MHz, and $\varepsilon_p/2\pi = 7$ MHz, respectively.

can confirm that the value of the minimum dip really decreases first and then increases with the increase of the coupling strength g_2. As can be shown in Figs. 5(e)–5(h), however, significant differences can be observed when compared with the case of $J = 0$. For $J \neq 0$, the depth of the first dip becomes deeper and deeper as the coupling strength g_2 varies from $0.3g_1$ to $0.9g_1$. This result is well reflected by the blue area in Fig. 6(b), where the blue color gradually deepens as g_2 increases. When the blue becomes deeper, the photon antibunching becomes stronger. Interestingly, the second dip becomes clearer when the interatomic DDI is considered, as shown in Figs. 5(e)–5(g). For example, in Fig. 5(e), there is a sharp dip that cannot be found in Figs. 5(a)–5(d) in the range of $\Delta > 0$, and the value of the second dip is about -0.33. Notice that the depth of the second dip in Figs. 5(e)–5(h) gets shallower and shallower with the increase of g_2, and it is almost invisible in Fig. 5(h). From Fig. 6(b), on the right side of $\Delta = 0$, this phenomenon can also be proved in the light green area. For the same g_2, the depths of the

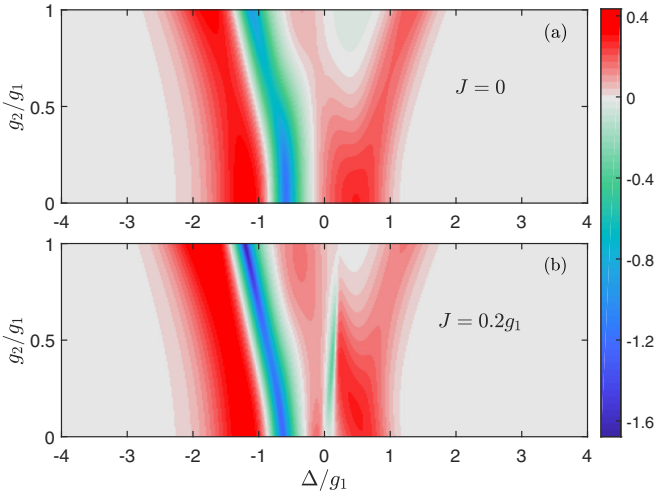

FIG. 6. Contour plot of the equal-time second-order correlation function of the cavity mode a on a logarithmic scale $\log_{10}[g_a^{(2)}(0)]$ as a function of the laser detuning Δ and the atom-cavity coupling strength g_2 under two different conditions: (a) without interatomic DDI strengths $J = 0$ and (b) with interatomic DDI strengths $J = 0.2g_1$ (i.e., $J/2\pi = 14$ MHz). The other system parameters used here are set as follows: $\kappa_{ia}/2\pi = \kappa_{ib}/2\pi = 75$ MHz, $\kappa_{ea}/2\pi = \kappa_{eb}/2\pi = 90$ MHz, $\Gamma_1/2\pi = \Gamma_2/2\pi = 5.2$ MHz, $\gamma_1/2\pi = \gamma_2/2\pi = 0$, $h/2\pi = 50$ MHz, $g_1/2\pi = 70$ MHz, and $\varepsilon_p/2\pi = 7$ MHz, respectively.

minimum dip in Figs. 5(e)–5(h) are always deeper than those in Figs. 5(a)–5(d), which once again tells us that the photon antibunching can be enhanced by considering the interatomic coupling.

So far, we have not yet taken into account the effect of the atomic dissipation induced by the DDI on the photon statistics of the system. In fact, the cooperative atomic decay does exist even though it is so small that it is always ignored. By assuming $\gamma_1 = \gamma_2 = \gamma$, Fig. 7 shows (a) the equal-time second-order correlation function on a logarithmic scale $\log_{10}[g_a^{(2)}(0)]$ and

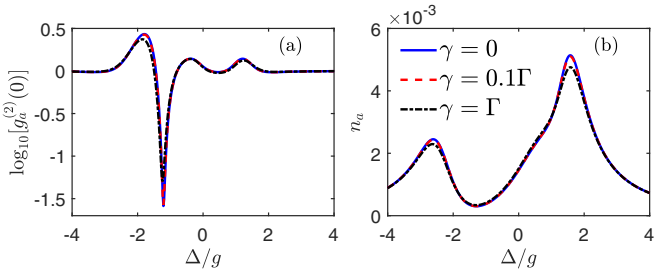

FIG. 7. (a) The equal-time second-order correlation functions on a logarithmic scale $\log_{10}[g_a^{(2)}(0)]$ and (b) the intracavity photon number n_a of the cavity mode a as a function of the laser detuning Δ for three different values of the cooperative atomic decay γ. The blue solid line, the red dashed line, and the black dot-dashed line in both panels represent the results with $\gamma = 0$, $\gamma = 0.1\Gamma$, and $\gamma = \Gamma$, respectively. The other system parameters used here are set as follows: $\kappa_{ia}/2\pi = \kappa_{ib}/2\pi = 75$ MHz, $\kappa_{ea}/2\pi = \kappa_{eb}/2\pi = 90$ MHz, $\Gamma_1/2\pi = \Gamma_2/2\pi = 5.2$ MHz, $h/2\pi = 50$ MHz, $g_1 = g_2 = g$, $g/2\pi = 70$ MHz, $J = 0.2g$, and $\varepsilon_p/2\pi = 7$ MHz, respectively.

(b) the intracavity photon number n_a of the cavity mode a, as a function of the laser detuning Δ for three different values of the cooperative atomic decay γ, respectively. It can be seen that both $\log_{10}[g_a^{(2)}(0)]$ and n_a are the red-blue detuning asymmetry. With increasing the cooperative atomic decay rate, neither the profile of $\log_{10}[g_a^{(2)}(0)]$ nor n_a has changed too much. For instance, when the cooperative atomic decay rate $\gamma = 0.1\Gamma$ (the red dashed line), the line shape of $\log_{10}[g_a^{(2)}(0)]$ (n_a) is almost coincident with the case of $\gamma = 0$ (the blue solid line). This indicates that the value of $\log_{10}[g_a^{(2)}(0)]$ (or n_a) is not sensitive to the cooperative atomic decay rate. As the cooperative atomic decay rate further increases (i.e., $\gamma = \Gamma$), the minimum dip of $\log_{10}[g_a^{(2)}(0)]$ rises slightly. Nevertheless, the qualitative nature of the photon antibunching is unchanged. The corresponding intracavity photon number n_a is still large, which can be treated as the single-photon regime. These observations reveal the extraordinary robustness of $\log_{10}[g_a^{(2)}(0)]$ (or n_a) against the cooperative atomic decay rate. Also, it is reasonable to assume $\gamma_1 = \gamma_2 = 0$ in the above discussion.

IV. CONCLUSIONS

In summary, we have theoretically studied the characteristics of photon correlation in a cavity QED architecture consisting of a bimodal WGM microresonator and two-level atoms for three different arrangements: (i) only one two-level atom, (ii) two far apart separated two-level atoms without interatomic DDI, and (iii) two dipole-coupled two-level atoms with interatomic DDI. We focus mainly on the effect of DDI on the photon antibunching of the system. By solving numerically the quantum master equation and using realistic experimental parameters, we have shown that the quality of the photon antibunching can be manipulated and enhanced by considering the interatomic coupling. Specifically, compared to the case that there are two two-level atoms without interatomic DDI, we have revealed that the enhanced photon antibunching can be achieved efficiently in the dipole-coupled atom-microresonator QED system. What is more, we also have found that the photon antibunching is stronger than the extensively studied case that only one two-level atom coupled to the bimodal WGM microresonator. The influence of the atom-cavity coupling strength on the photon antibunching is discussed as well in detail. When DDI between the two two-level atoms exists, it is shown that the photon antibunching can be optimized by properly adjusting the atom-cavity coupling strength whether the coupling coefficients of the two atoms to the microresonator are the same or not. Finally, it is demonstrated that the extraordinary robustness of the steady-state second-order correlation function and the intracavity photon number against the cooperative atomic decay rate, which is induced by the interatomic DDI, can appear. Because all the obtained results are based on readily available experimental parameters, our DDI-based cavity QED investigation may be useful for the construction of integrated on-chip single-photon sources.

Alternatively, as a remark, it is worth mentioning that a few different platforms can be used in the present investigation for the realization of integrated single-photon sources. For example, lithium niobate, dubbed by many as the silicon

of photonics, has become a promising candidate for an integrated photonic platform [99–107]. Due to its beneficial properties that include strong quadratic optical nonlinearity ($\chi^{(2)} = 30$ pm/V [99]), a wide transparency window, large piezoelectric response, high refractive index, as well as recent advances in the development of a low-loss thin-film lithium niobate on an insulator platform, lithium niobate is particularly attractive and widely used in optical and microwave technologies [99–101]. Given that the lithium niobate is a second-order nonlinear optical material, the lithium niobate WGM microresonators of a ultra-low loss and ultra-high quality factor may bring nonlinear systems into a new design parameter space and more colorful quantum phenomena [99–102,104,106,107]. The state-of-the-art technology to manufacture the WGM microresonators made of lithium niobate is mature. The high quality factor and small mode volume of the fabricated lithium niobate WGM microresonators also have been successfully reported in experiments [99,100,102]. It follows that, by the appropriate design of optical elements, this lithium niobate platform can be implemented into our present model. As a consequence, it would be very instructive to explore the characteristics of the photon antibunching based on these chip-integrated lithium niobate WGM microresonators and further compare the antibunching with what would be expected in lithium niobite (second-order material). Such an analysis is, however, beyond the scope of the current work, and we plan to address this problem in the near future.

ACKNOWLEDGMENTS

We wish to thank the anonymous referees for their valuable and insightful comments. We also acknowledge the enlightening discussions with Xiaoxue Yang and Rong Yu during the manuscript preparation. Y.Q., S.S., and J.L. are supported in part by the National Natural Science Foundation of China under Grant No. 11675058 and the Fundamental Research Funds for the Central Universities (Huazhong University of Science and Technology) under Grant No. 2018KFYYXJJ037. Y.W. is supported in part by the National Key Research and Development Program of China under Grant No. 2016YFA0301200 as well as the National Natural Science Foundation of China under Grants No. 11875029 and No. 11574104.

APPENDIX: INSIGHTS INTO THE SECOND-ORDER CORRELATION FUNCTION IN THE WEAK-DRIVING LIMIT VIA A SCHRÖDINGER EQUATION APPROACH

In order to have a better understanding of numerical calculation, we undertake an analytical discussion about the photon correlation. Under the condition that the external driving laser field is very weak $\varepsilon_p \ll \kappa_a$ and κ_b, the total excitation number of the system is no more than two [26,31,71]. The two two-level atoms are initially in the ground state. In this circumstance, the quantum state of the whole system can be written as

$$\begin{aligned}|\psi\rangle = {} & C_{00gg}|0,0,g,g\rangle + C_{10gg}|1,0,g,g\rangle + C_{01gg}|0,1,g,g\rangle \\ & + C_{00ge}|0,0,g,e\rangle + C_{00eg}|0,0,e,g\rangle + C_{20gg}|2,0,g,g\rangle \\ & + C_{02gg}|0,2,g,g\rangle + C_{11gg}|1,1,g,g\rangle + C_{10ge}|1,0,g,e\rangle \\ & + C_{10eg}|1,0,e,g\rangle + C_{01ge}|0,1,g,e\rangle + C_{01eg}|0,1,e,g\rangle,\end{aligned} \tag{A1}$$

where the coefficients $C_{n_a n_b n_1 n_2}$ (with $n_a = 0, 1, 2$ photons in the cavity mode a; $n_b = 0, 1, 2$ photons in the cavity mode b; $n_1 = |g\rangle$, $|e\rangle$ states in the first two-level atom; and $n_2 = |g\rangle$, $|e\rangle$ states in the second two-level atom) are the amplitudes of the corresponding quantum states $|n_a, n_b, n_1, n_2\rangle$. In the weak-driving limit $\varepsilon_p \ll \kappa_a$, we have

$$\begin{aligned}|C_{00gg}| \gg |C_{10gg}|, |C_{01gg}|, |C_{00ge}|, |C_{00eg}| \gg |C_{20gg}|, |C_{02gg}|, \\ |C_{11gg}|, |C_{10ge}|, |C_{10eg}|, |C_{01ge}|, |C_{01eg}|.\end{aligned} \tag{A2}$$

Using the relationship in Eq. (A2) and combining with Eqs. (12) and (A1), the equal-time second-order correlation function $g_a^{(2)}(0)$ can be approximately expressed as

$$g_a^{(2)}(0) \approx \frac{2|C_{20gg}|^2}{|C_{10gg}|^4}. \tag{A3}$$

To obtain the coefficients C_{20gg} and C_{10gg}, we can solve the Schrödinger equation

$$i\hbar\frac{\partial|\psi\rangle}{\partial t} = \widetilde{\mathcal{H}}|\psi\rangle \tag{A4}$$

with the effective non-Hermitian Hamiltonian including the cavity-mode decay and two-level atomic damping terms together with the original Hamiltonian term (4), namely,

$$\begin{aligned}\widetilde{\mathcal{H}} = {} & \mathcal{H} - i\frac{\kappa_a}{2}a^\dagger a - i\frac{\kappa_b}{2}b^\dagger b \\ & - i\frac{\Gamma_1+\gamma_{12}}{2}\sigma_1^\dagger\sigma_1 - i\frac{\Gamma_2+\gamma_{21}}{2}\sigma_2^\dagger\sigma_2.\end{aligned} \tag{A5}$$

In the steady state, $\partial|\psi\rangle/\partial t = 0$, a set of coupled linear equations for the coefficients $C_{n_a n_b n_1 n_2}$ can be obtained after some lengthy but straightforward calculations, with the forms

$$\begin{aligned}0 = {} & \bar{\Delta}_C C_{10gg} + g_1 C_{00eg} + g_2 C_{00ge} + hC_{01gg} \\ & + \sqrt{2}\varepsilon_p C_{20gg} + \varepsilon_p,\end{aligned} \tag{A6}$$

$$0 = \bar{\Delta}_C C_{01gg} + g_1 C_{00eg} + g_2 C_{00ge} + hC_{10gg} + \varepsilon_p C_{11gg}, \tag{A7}$$

$$0 = \bar{\Delta}_A C_{00ge} + g_2(C_{10gg} + C_{01gg}) + JC_{00eg} + \varepsilon_p C_{10ge}, \tag{A8}$$

$$0 = \bar{\Delta}_A C_{00eg} + g_1(C_{10gg} + C_{01gg}) + JC_{00ge} + \varepsilon_p C_{10eg}, \tag{A9}$$

$$\begin{aligned}0 = {} & 2\bar{\Delta}_C C_{20gg} + \sqrt{2}g_1 C_{10eg} + \sqrt{2}g_2 C_{10ge} \\ & + \sqrt{2}hC_{11gg} + \sqrt{2}\varepsilon_p C_{10gg},\end{aligned} \tag{A10}$$

$$0 = 2\bar{\Delta}_C C_{02gg} + \sqrt{2}g_1 C_{01eg} + \sqrt{2}g_2 C_{01ge} + \sqrt{2}hC_{11gg}, \tag{A11}$$

$$0 = 2\bar{\Delta}_C C_{11gg} + g_1(C_{01eg} + C_{10eg}) + g_2(C_{01ge} + C_{10ge}) + \sqrt{2}h(C_{20gg} + C_{02gg}) + \varepsilon_p C_{01gg}, \tag{A12}$$

$$0 = (\bar{\Delta}_C + \bar{\Delta}_A)C_{10ge} + g_2 C_{11gg} + \sqrt{2}g_2 C_{20gg} + hC_{01ge} + JC_{10eg} + \varepsilon_p C_{00ge}, \tag{A13}$$

$$0 = (\bar{\Delta}_C + \bar{\Delta}_A)C_{10eg} + g_1 C_{11gg} + \sqrt{2}g_1 C_{20gg} + hC_{01eg} + JC_{10ge} + \varepsilon_p C_{00eg}, \tag{A14}$$

$$0 = (\bar{\Delta}_C + \bar{\Delta}_A)C_{01ge} + g_2 C_{11gg} + \sqrt{2}g_2 C_{02gg} + hC_{10ge} + JC_{01eg}, \tag{A15}$$

$$0 = (\bar{\Delta}_C + \bar{\Delta}_A)C_{01eg} + g_1 C_{11gg} + \sqrt{2}g_1 C_{02gg} + hC_{10eg} + JC_{01ge}, \tag{A16}$$

where $\bar{\Delta}_C = \Delta - i\frac{\kappa}{2}$ and $\bar{\Delta}_A = \Delta - i\frac{\Gamma+\gamma}{2}$. Here we have considered $\kappa_a = \kappa_b = \kappa$, $\Gamma_1 = \Gamma_2 = \Gamma$, and $\gamma_{12} = \gamma_{21} = \gamma$. Alternatively, due to the weak-driving limit and in the steady state, we can assume $C_{00gg} \to 1$ as in Refs. [31,71], and one additional equation, namely, $\varepsilon_p C_{10gg} = 0$, is irrelevant to the problem. Obviously, these coupled algebraic equations (A6)–(A16) are closed (i.e., 11 equations for 11 parameters). Thus, in principle, a complete solution for the coefficients $C_{n_a n_b n_1 n_2}$ and the corresponding second-order correlation function $g_a^{(2)}(0)$ can be obtained by directly solving the above coupled algebraic equations. However, the solutions are too tedious to be included here. From the above derivation results, we can find the second-order correlation function $g_a^{(2)}(0)$ is associated to the mode-coupling strength h, the atom-cavity coupling g_k, and the DDI coefficient J between the two two-level atoms. In the current work, we are more interested in the effect of interatomic DDI on the photon antibunching for the coherently coupled atom-microresonator compound system. The corresponding analytical results have been validated by the above numerical calculations.

[1] V. Giovannetti, S. Lloyd, and L. Maccone, Quantum Metrology, Phys. Rev. Lett. **96**, 010401 (2006).

[2] E. Knill, R. Laflamme, and G. J. Milburn, A scheme for efficient quantum computation with linear optics, Nature (London) **409**, 46 (2001).

[3] T. Jennewein, M. Barbieri, and A. G. White, Single-photon device requirements for operating linear optics quantum computing outside the post-selection basis, J. Mod. Opt. **58**, 276 (2011).

[4] I. Buluta and F. Nori, Quantum simulators, Science **326**, 108 (2009).

[5] I. M. Georgescu, S. Ashhab, and F. Nori, Quantum simulation, Rev. Mod. Phys. **86**, 153 (2014).

[6] A. Kuhn, M. Hennrich, and G. Rempe, Deterministic Single-Photon Source for Distributed Quantum Networking, Phys. Rev. Lett. **89**, 067901 (2002).

[7] H. Wang, Y. M. He, T. H. Chung, H. Hu, Y. Yu, S. Chen, X. Ding, M. C. Chen, J. Qin, X. X. Yang, R. Z. Liu, Z. C. Duan, J. P. Li, S. Gerhardt, K. Winkler, J. Jurkat, L. J. Wang, N. Gregersen, Y. H. Huo, Q. Dai, S. Y. Yu, S. Höfling, C. Y. Lu, and J. W. Pan, Towards optimal single-photon sources from polarized microcavities, Nat. Photonics **13**, 770 (2019).

[8] K. M. Birnbaum, A. Boca, R. Miller, A. D. Boozer, T. E. Northup, and H. J. Kimble, Photon blockade in an optical cavity with one trapped atom, Nature (London) **436**, 87 (2005).

[9] B. Dayan, A. S. Parkins, T. Aoki, E. P. Ostby, K. J. Vahala, and H. J. Kimble, A photon turnstile dynamically regulated by one atom, Science **319**, 1062 (2008).

[10] A. Faraon, I. Fushman, D. Englund, N. Stoltz, P. Petroff, and J. Vučković, Coherent generation of non-classical light on a chip via photon-induced tunnelling and blockade, Nat. Phys. **4**, 859 (2008).

[11] A. Reinhard, T. Volz, M. Winger, A. Badolato, K. J. Hennessy, E. L. Hu, and A. Imamolu, Strongly correlated photons on a chip, Nat. Photonics **6**, 93 (2012).

[12] C. Hamsen, K. N. Tolazzi, T. Wilk, and G. Rempe, Two-Photon Blockade in an Atom-Driven Cavity QED System, Phys. Rev. Lett. **118**, 133604 (2017).

[13] For recent reviews, see M. Radulaski, K. Fischer, and J. Vučković, Nonclassical light generation from III-V and group-IV solid-state cavity quantum systems, Adv. At. Mol. Opt. Phys. **66**, 111 (2017).

[14] W. W. Deng, G. X. Li, and H. Qin, Enhancement of the two-photon blockade in a strong-coupling qubit-cavity system, Phys. Rev. A **91**, 043831 (2015).

[15] Y. H. Zhou, H. Z. Shen, X. Y. Zhang, and X. X. Yi, Zero eigenvalues of a photon blockade induced by a non-Hermitian Hamiltonian with a gain cavity, Phys. Rev. A **97**, 043819 (2018).

[16] P. Rabl, Photon Blockade Effect in Optomechanical Systems, Phys. Rev. Lett. **107**, 063601 (2011).

[17] A. Nunnenkamp, K. Børkje, and S. M. Girvin, Single-Photon Optomechanics, Phys. Rev. Lett. **107**, 063602 (2011).

[18] C. Lang, D. Bozyigit, C. Eichler, L. Steffen, J. M. Fink, A. A. Abdumalikov, Jr., M. Baur, S. Filipp, M. P. da Silva, A. Blais, and A. Wallraff, Observation of Resonant Photon Blockade at Microwave Frequencies Using Correlation Function Measurements, Phys. Rev. Lett. **106**, 243601 (2011).

[19] A. J. Hoffman, S. J. Srinivasan, S. Schmidt, L. Spietz, J. Aumentado, H. E. Türeci, and A. A. Houck, Dispersive Photon Blockade in a Superconducting Circuit, Phys. Rev. Lett. **107**, 053602 (2011).

[20] Y. X. Liu, X. W. Xu, A. Miranowicz, and F. Nori, From blockade to transparency: Controllable photon transmission through a circuit-QED system, Phys. Rev. A **89**, 043818 (2014).

[21] J. T. Shen and S. H. Fan, Strongly Correlated Two-Photon Transport in a One-Dimensional Waveguide Coupled to a Two-Level System, Phys. Rev. Lett. **98**, 153003 (2007).

[22] S. Mahmoodian, M. Čepulkovskis, S. Das, P. Lodahl, K. Hammerer, and A. S. Sørensen, Strongly Correlated Photon Transport in Waveguide Quantum Electrodynamics with Weakly Coupled Emitters, Phys. Rev. Lett. **121**, 143601 (2018).

[23] A. Miranowicz, J. Bajer, M. Paprzycka, Y. X. Liu, A. M. Zagoskin, and F. Nori, State-dependent photon blockade via

quantum-reservoir engineering, Phys. Rev. A **90**, 033831 (2014).
[24] R. Huang, A. Miranowicz, J.-Q. Liao, F. Nori, and H. Jing, Nonreciprocal Photon Blockade, Phys. Rev. Lett. **121**, 153601 (2018).
[25] T. C. H. Liew and V. Savona, Single Photons from Coupled Quantum Modes, Phys. Rev. Lett. **104**, 183601 (2010).
[26] M. Bamba, A. Imamoğlu, I. Carusotto, and C. Ciuti, Origin of strong photon antibunching in weakly nonlinear photonic molecules, Phys. Rev. A **83**, 021802 (2011).
[27] A. Majumdar, M. Bajcsy, A. Rundquist, and J. Vučković, Loss-Enabled Sub-Poissonian Light Generation in a Bimodal Nanocavity, Phys. Rev. Lett. **108**, 183601 (2012).
[28] H. Flayac and V. Savona, Input-output theory of the unconventional photon blockade, Phys. Rev. A **88**, 033836 (2013).
[29] X. W. Xu and Y. Li, Tunable photon statistics in weakly nonlinear photonic molecules, Phys. Rev. A **90**, 043822 (2014).
[30] H. Flayac and V. Savona, Unconventional photon blockade, Phys. Rev. A **96**, 053810 (2017).
[31] C. Q. Wang, Y. L. Liu, R. B. Wu, and Y. X. Liu, Phase-modulated photon antibunching in a two-level system coupled to two cavities, Phys. Rev. A **96**, 013818 (2017).
[32] B. Li, R. Huang, X. Xu, A. Miranowicz, and H. Jing, Nonreciprocal unconventional photon blockade in a spinning optomechanical system, Photon. Res. **7**, 630 (2019).
[33] D. Gerace and V. Savona, Unconventional photon blockade in doubly resonant microcavities with second-order nonlinearity, Phys. Rev. A **89**, 031803 (2014).
[34] Y. H. Zhou, H. Z. Shen, and X. X. Yi, Unconventional photon blockade with second-order nonlinearity, Phys. Rev. A **92**, 023838 (2015).
[35] H. Flayac and V. Savona, Single photons from dissipation in coupled cavities, Phys. Rev. A **94**, 013815 (2016).
[36] H. Z. Shen, Y. H. Zhou, and X. X. Yi, Tunable photon blockade in coupled semiconductor cavities, Phys. Rev. A **91**, 063808 (2015).
[37] X. W. Xu and Y. Li, Strong photon antibunching of symmetric and antisymmetric modes in weakly nonlinear photonic molecules, Phys. Rev. A **90**, 033809 (2014).
[38] A. Miranowicz, J. Bajer, N. Lambert, Y. X. Liu, and F. Nori, Tunable multiphonon blockade in coupled nanomechanical resonators, Phys. Rev. A **93**, 013808 (2016).
[39] J. H. Li and Y. Wu, Quality of photon antibunching in two cavity-waveguide arrangements on a chip, Phys. Rev. A **98**, 053801 (2018).
[40] C. Vaneph, A. Morvan, G. Aiello, M. Féchant, M. Aprili, J. Gabelli, and J. Estève, Observation of the Unconventional Photon Blockade in the Microwave Domain, Phys. Rev. Lett. **121**, 043602 (2018).
[41] H. J. Snijders, J. A. Frey, J. Norman, H. Flayac, V. Savona, A. C. Gossard, J. E. Bowers, M. P. van Exter, D. Bouwmeester, and W. Löffler, Observation of the Unconventional Photon Blockade, Phys. Rev. Lett. **121**, 043601 (2018).
[42] Q. A. Turchette, C. J. Hood, W. Lange, H. Mabuchi, and H. J. Kimble, Measurement of Conditional Phase Shifts for Quantum Logic, Phys. Rev. Lett. **75**, 4710 (1995).
[43] M. Hennrich, A. Kuhn, and G. Rempe, Transition from Antibunching to Bunching in Cavity QED, Phys. Rev. Lett. **94**, 053604 (2005).
[44] A. B. Matsko and V. S. Ilchenko, Optical resonators with whispering-gallery modes—Part I: Basics, IEEE J. Sel. Top. Quantum Electron. **12**, 3 (2006).
[45] V. S. Ilchenko and A. B. Matsko, Optical resonators with whispering-gallery modes—Part II: Applications, IEEE J. Sel. Top. Quantum Electron. **12**, 15 (2006).
[46] O. Painter, R. K. Lee, A. Scherer, A. Yariv, J. D. O'Brien, P. D. Dapkus, and I. Kim, Two-dimensional photonic band-gap defect mode laser, Science **284**, 1819 (1999).
[47] J. Vučković, Quantum optics and cavity QED with quantum dots in photonic crystals, in *Quantum Optics and Nanophotonics*, edited by C. Fabre, V. Sandoghdar, N. Treps, and L. F. Cugliandolo (Oxford University Press, Oxford, 2017), pp. 365–406.
[48] T. Aoki, B. Dayan, E. Wilcut, W. P. Bowen, A. S. Parkins, T. J. Kippenberg, K. J. Vahala, and H. J. Kimble, Observation of strong coupling between one atom and a monolithic microresonator, Nature (London) **443**, 671 (2006).
[49] T. Aoki, A. S. Parkins, D. J. Alton, C. A. Regal, B. Dayan, E. Ostby, K. J. Vahala, and H. J. Kimble, Efficient Routing of Single Photons by One Atom and a Microtoroidal Cavity, Phys. Rev. Lett. **102**, 083601 (2009).
[50] V. S. Ilchenko, A. A. Savchenkov, A. B. Matsko, and L. Maleki, Nonlinear Optics and Crystalline Whispering Gallery Mode Cavities, Phys. Rev. Lett. **92**, 043903 (2004).
[51] T. J. Kippenberg and K. J. Vahala, Cavity optomechanics: Back-action at the mesoscale, Science **321**, 1172 (2008).
[52] M. Aspelmeyer, Cavity optomechanics, Rev. Mod. Phys. **86**, 1391 (2014).
[53] H. Cao and J. Wiersig, Dielectric microcavities: Model systems for wave chaos and non-Hermitian physics, Rev. Mod. Phys. **87**, 61 (2015).
[54] X. F. Jiang, L. B. Shao, S. X. Zhang, X. Yi, J. Wiersig, L. Wang, Q. H. Gong, M. Lončar, L. Yang, and Y. F. Xiao, Chaos-assisted broadband momentum transformation in optical microresonators, Science **358**, 344 (2017).
[55] A. M. Armani and K. J. Vahala, Heavy water detection using ultra-high-Q microcavities, Opt. Lett. **31**, 1896 (2006).
[56] B. Q. Shen, X. C. Yu, Y. Zhi, L. Wang, D. Kim, Q. Gong, and Y. F. Xiao, Detection of Single Nanoparticles using the Dissipative Interaction in a High-Q Microcavity, Phys. Rev. Appl. **5**, 024011 (2016).
[57] F. Vollmer, D. Braun, A. Libchaber, M. Khoshsima, I. Teraoka, and S. Arnold, Protein detection by optical shift of a resonant microcavity, Appl. Phys. Lett. **80**, 4057 (2002).
[58] N. M. Hanumegowda, C. J. Stica, B. C. Patel, I. White, and X. Fan, Refractometric sensors based on microsphere resonators, Appl. Phys. Lett. **87**, 201107 (2005).
[59] C. Y. Chao, W. Fung, and L. J. Guo, Polymer microring resonators for biochemical sensing applications, IEEE J. Sel. Top. Quantum Electron. **12**, 134 (2006).
[60] H. Zhu, I. M. White, J. D. Suter, P. S. Dale, and X. Fan, Analysis of biomolecule detection with optofluidic ring resonator sensors, Opt. Express **15**, 9139 (2007).
[61] M. Sumetsky, R. S. Windeler, Y. Dulashko, and X. Fan, Optical liquid ring resonator sensor, Opt. Express **15**, 14376 (2007).
[62] S. Li, L. Ma, S. Böttner, Y. Mei, M. R. Jorgensen, S. Kiravittaya, and O. G. Schmidt, Angular position detection

of single nanoparticles on rolled-up optical microcavities with lifted degeneracy, Phys. Rev. A **88**, 033833 (2013).

[63] M. Sumetsky, Y. Dulashko, and R. S. Windeler, Optical microbubble resonator, Opt. Lett. **35**, 898 (2010).

[64] Y. Yang, J. Ward, and S. N. Chormaic, Quasi-droplet microbubbles for high resolution sensing applications, Opt. Express **22**, 6881 (2014).

[65] J. Kim, M. C. Kuzyk, K. Han, H. Wang, and G. Bahl, Non-reciprocal Brillouin scattering induced transparency, Nat. Phys. **11**, 275 (2015).

[66] Z. Shen, Y. L. Zhang, Y. Chen, C. L. Zou, Y. F. Xiao, X. B. Zou, F. W. Sun, G. C. Guo, and C. H. Dong, Experimental realization of optomechanically induced non-reciprocity, Nat. Photon. **10**, 657 (2016).

[67] L. Chang, X. Jiang, S. Hua, C. Yang, J. Wen, L. Jiang, G. Li, G. Wang, and M. Xiao, Parity-time symmetry and variable optical isolation in active-passive-coupled microresonators, Nat. Photon. **8**, 524 (2014).

[68] B. Peng, S. K. Özdemir, F. Lei, F. Monifi, M. Gianfreda, G. L. Long, S. Fan, F. Nori, C. M. Bender, and L. Yang, Parity-time-symmetric whispering-gallery microcavities, Nat. Phys. **10**, 394 (2014).

[69] W. Chen, S. Ozdemir, G. Zhao, J. Wiersig, and L. Yang, Exceptional points enhance sensing in an optical microcavity, Nature (London) **548**, 192 (2017).

[70] Y. K. Lu, P. Peng, Q. T. Cao, D. Xu, J. Wiersig, Q. Gong, and Y. F. Xiao, Spontaneous $\mathcal{T}$-symmetry breaking and exceptional points in cavity quantum electrodynamics systems, Sci. Bull. **63**, 1096 (2018).

[71] Y. L. Liu, G. Z. Wang, Y. X. Liu, and F. Nori, Mode coupling and photon antibunching in a bimodal cavity containing a dipole quantum emitter, Phys. Rev. A **93**, 013856 (2016).

[72] G. K. Brennen, I. H. Deutsch, and P. S. Jessen, Entangling dipole-dipole interactions for quantum logic with neutral atoms, Phys. Rev. A **61**, 062309 (2000).

[73] S. Nicolosi, A. Napoli, A. Messina, and F. Petruccione, Dissipation-induced stationary entanglement in dipole-dipole interacting atomic samples, Phys. Rev. A **70**, 022511 (2004).

[74] N. B. An, J. Kim, and K. Kim, Entanglement dynamics of three interacting two-level atoms within a common structured environment, Phys. Rev. A **84**, 022329 (2011).

[75] Q. H. Chen, T. Liu, Y. Y. Zhang, and K. L. Wang, Quantum phase transitions in coupled two-level atoms in a single-mode cavity, Phys. Rev. A **82**, 053841 (2010).

[76] L. Tan, Y. Q. Zhang, and W. M. Liu, Quantum phase transitions for two coupled cavities with dipole-interaction atoms, Phys. Rev. A **84**, 063816 (2011).

[77] Y. Q. Zhang, L. Tan, and P. Barker, Effects of dipole-dipole interaction on the transmitted spectrum of two-level atoms trapped in an optical cavity, Phys. Rev. A **89**, 043838 (2014).

[78] S. Weis, R. Rivière, S. Deléglise, E. Gavartin, O. Arcizet, A. Schliesser, and T. J. Kippenberg, Optomechanically induced transparency, Science **330**, 1520 (2010).

[79] S. M. Spillane, T. J. Kippenberg, O. J. Painter, and K. J. Vahala, Ideality in a Fiber-Taper-Coupled Microresonator System for Application to Cavity Quantum Electrodynamics, Phys. Rev. Lett. **91**, 043902 (2003).

[80] S. Welte, B. Hacker, S. Daiss, S. Ritter, and G. Rempe, Photon-Mediated Quantum Gate between Two Neutral Atoms in an Optical Cavity, Phys. Rev. X **8**, 011018 (2018).

[81] N. Schlosser, G. Reymond, I. Protsenko, and P. Grangier, Sub-Poissonian loading of single atoms in a microscopic dipole trap, Nature (London) **411**, 1024 (2001).

[82] J. Beugnon, C. Tuchendler, H. Marion, A. Gaëtan, Y. Miroshnychenko, Y. R. P. Sortais, A. M. Lance, M. P. A. Jones, G. Messin, A. Browaeys, and P. Grangier, Two-dimensional transport and transfer of a single atomic qubit in optical tweezers, Nat. Phys. **3**, 696 (2007).

[83] J. D. Thompson, T. G. Tiecke, A. S. Zibrov, V. Vuletić, and M. D. Lukin, Coherence and Raman Sideband Cooling of a Single Atom in an Optical Tweezer, Phys. Rev. Lett. **110**, 133001 (2013).

[84] M. G. Raizen, R. J. Thompson, R. J. Brecha, H. J. Kimble, and H. J. Carmichael, Normal-Mode Splitting and Linewidth Averaging for Two-State Atoms in an Optical Cavity, Phys. Rev. Lett. **63**, 240 (1989).

[85] G. Rempe, R. J. Thompson, R. J. Brecha, W. D. Lee, and H. J. Kimble, Optical Bistability and Photon Statistics in Cavity Quantum Electrodynamics, Phys. Rev. Lett. **67**, 1727 (1991).

[86] R. J. Thompson, G. Rempe, and H. J. Kimble, Observation of Normal-Mode Splitting for an Atom in an Optical Cavity, Phys. Rev. Lett. **68**, 1132 (1992).

[87] J. Pellegrino, R. Bourgain, S. Jennewein, Y. R. P. Sortais, and A. Browaeys, Observation of Suppression of Light Scattering Induced by Dipole-Dipole Interactions in a Cold-Atom Ensemble, Phys. Rev. Lett. **113**, 133602 (2014).

[88] M. T. Cheng, J. P. Xu, and G. S. Agarwal, Waveguide transport mediated by strong coupling with atoms, Phys. Rev. A **95**, 053807 (2017).

[89] H. J. Carmichael, *An Open Systems Approach to Quantum Optics*, Lecture Notes in Physics Vol. 18 (Springer-Verlag, Berlin, 1993).

[90] M. L. Gorodetsky, A. D. Pryamikov, and V. S. Ilchenko, Rayleigh scattering in high-Q microspheres, J. Opt. Soc. Am. B **17**, 1051 (2010).

[91] S. M. Spillane, T. J. Kippenberg, and K. J. Vahala, Ultrahigh-Q toroidal microresonators for cavity quantum electrodynamics, Phys. Rev. A **71**, 013817 (2005).

[92] A. F. Alharbi and Z. Ficek, Deterministic creation of stationary entangled states by dissipation, Phys. Rev. A **82**, 054103 (2010).

[93] R. H. Brown and R. Q. Twiss, A test of a new type of stellar interferometer on Sirius, Nature (London) **178**, 1046 (1956).

[94] U. Fano, On the absorption spectrum of noble gases at the arc spectrum limit, Nuovo Cimento **12**, 154 (1935).

[95] U. Fano, Effects of configuration interaction on intensities and phase shifts, Phys. Rev. **124**, 1866 (1961).

[96] S. B. Zheng and G. C. Guo, Efficient Scheme for Two-Atom Entanglement and Quantum Information Processing in Cavity QED, Phys. Rev. Lett. **85**, 2392 (2000).

[97] S. Natali and Z. Ficek, Temporal and diffraction effects in entanglement creation in an optical cavity, Phys. Rev. A **75**, 042307 (2007).

[98] S. Maniscalco, F. Francica, R. L. Zaffino, N. L. Gullo, and F. Plastina, Protecting Entanglement via the Quantum Zeno Effect, Phys. Rev. Lett. **100**, 090503 (2008).

[99] M. Zhang, C. Wang, R. Cheng, A. Shams-Ansari, and M. Loncar, Monolithic ultra-high-Q lithium niobate microring resonator, Optica **4**, 1536 (2017).

[100] R. Wu, J. Zhang, N. Yao, W. Fang, L. Qiao, Z. Chai, J. Lin, and Y. Cheng, Lithium niobate micro-disk resonators of quality factors above 10^7, Opt. Lett. **43**, 4116 (2018).

[101] J. J. Lu, J. B. Surya, X. W. Liu, A. W. Bruch, Z. Gong, Y. T. Xu, and H. X. Tang, Periodically poled thin-film lithium niobate microring resonators with a second-harmonic generation efficiency of 250,000%/W, Optica **6**, 1455 (2019).

[102] R. Luo, Y. He, H. X. Liang, M. X. Li, J. W. Ling, and Q. Lin, Optical Parametric Generation in a Lithium Niobate Microring with Modal Phase Matching, Phys. Rev. Appl. **11**, 034026 (2019).

[103] C. Wang, M. Zhang, M. J. Yu, R. R. Zhu, H. Hu, and M. Loncar, Monolithic lithium niobate photonic circuits for Kerr frequency comb generation and modulation, Nat. Commun. **10**, 978 (2019).

[104] M. Zhang, B. Buscaino, C. Wang, A. Shams-Ansari, C. Reimer, R. R. Zhu, J. M. Kahn, and M. Lončar, Broadband electro-optic frequency comb generation in a lithium niobate microring resonator, Nature (London) **568**, 373 (2019).

[105] B. Desiatov, A. Shams-Ansari, M. Zhang, C. Wang, and M. Lonar, Ultra-low-loss integrated visible photonics using thin-film lithium niobate, Optica **6**, 380 (2019).

[106] J. T. Lin, N. Yao, Z. Z. Hao, J. H. Zhang, W. B. Mao, M. Wang, W. Chu, R. B. Wu, Z. W. Fang, L. L. Qiao, W. Fang, F. Bo, and Y. Cheng, Broadband Quasi-Phase-Matched Harmonic Generation in an On-Chip Monocrystalline Lithium Niobate Microdisk Resonator, Phys. Rev. Lett. **122**, 173903 (2019).

[107] J. Y. Chen, Z. H. Ma, Y. M. Sua, Z. Li, C. Tang, and Y. P. Huang, Ultra-efficient frequency conversion in quasi-phase-matched lithium niobate microrings, Optica **6**, 1244 (2019).